Aldol Condensation of *n*-Butyraldehyde in a Biphasic Stirred Tank Reactor: Experiments and Models

Shinbeom Lee and Arvind Varma
School of Chemical Engineering, Purdue University, 480 Stadium Mall Drive, West Lafayette, IN 47907

DOI 10.1002/aic.14817
Published online April 13, 2015 in Wiley Online Library (wileyonlinelibrary.com)

To model a biphasic stirred tank reactor, intrinsic reaction kinetics and interfacial area are required. In this study, reactor modeling for n-butyraldehyde aldol condensation was investigated under industrially relevent conditions. The interfacial area in the reactor was directly measured using a borescope system under appropriate temperature, NaOH concentration and rpm conditions. To estimate the interfacial area, a semiempirical correlation was developed, which provides good estimates within ±15% error. The reactor model based on two-film theory was developed, combining the interfacial area and intrinsic reaction kinetics reported in our prior work. The model was verified by reaction experiments in the range 0.05–1.9 M NaOH, 80–130°C, and 600–1000 rpm. The prediction errors using the interfacial area from direct measurements and the correlation were ±8% and ±15%, respectively, suggesting that the model accuracy may be improved with better interfacial area estimation. © 2015 American Institute of Chemical Engineers *AIChE J*, 61: 2228–2239, 2015
Keywords: biphasic reactor modeling, stirred tank reactor, interfacial area, aldol condensation, n-butyraldehyde

Introduction

Biphasic (liquid-liquid) reaction processes provide several advantages over other types, including low pressure drop, intimate catalyst–substrate mixing, high yield and selectivity, and ease of catalyst recycling.[1,2] For these reasons, biphasic reactions such as olefin alkylation, aromatic nitration, and alkaline hydrolysis are widely used in the refinery, petrochemical, fine chemical, and pharmaceutical industries.[3–5] Despite the prevalence of biphasic reactions in industry, little fundamental work has been performed to clarify coupled reaction-transport events in biphasic systems.[6] Investigation of these issues and development of reactor models which account for hydrodynamic and transport effects is essential for design and scale-up of biphasic reactors.

Successful reactor modeling requires the knowledge of intrinsic reaction kinetics and its coupling with transport phenomena.[7] A biphasic reactor contains two immiscible liquids with liquid-phase catalysts. One phase, primarily organic phase, includes the reactant feed and the other phase, mainly aqueous phase, includes catalysts such as acid–base or organometallic catalysts.[8] Based on the reaction rate, there are three different regimes to understand the phenomena in the aqueous phase, where the reaction occurs.[9,10] The Hatta number (*Ha*), which is the ratio of the reaction rate in the liquid film to the diffusion rate through the film,[11] is used as a criterion to characterize the regimes. If the reaction is fast ($Ha > 3$), all reactions occur in the film region of the aqueous phase and none in the bulk region; this is called the mass transfer controlled regime dominated by the reaction rate in the film.[12] Under these conditions, the Danckwerts penetration model[13] is preferred to estimate the reaction rate in the film.[14] For intermediate rates, reactions occur in both the film and the bulk regions because the reactant concentration in the bulk region is nonzero. In this regime, Quadros *et al.*[10] used the film model for benzene nitration in a continuous-flow stirred tank reactor. The penetration model may not be appropriate in this case due to the difficulty in determining the bulk-phase reactant concentration. In the third regime where the reaction is slow, there is no film resistance and the overall reaction rate is determined only by its intrinsic kinetics; this is called the reaction controlled regime.[15] In the cases of fast and intermediate reaction rates, knowledge of both interfacial reaction kinetics and interfacial area are required to understand the reactor behavior. However, determining the models and parameters describing these phenomena is challenging due to mass transfer disguised kinetics and difficulties in measurement and estimation of the interfacial area.

To evaluate these effects, a suitable reaction must be considered. Base-catalyzed biphasic aldol condensation of normal-butyraldehyde (nBAL) is conducted at the industrial operating conditions of 80–140°C, ~5 bar, with 2–4 wt % of sodium hydroxide (NaOH) as catalyst.[16] This reaction is a part of the oxo-alcohol process to produce 2-ethyl-1-hexanol (2EH) which is commonly used to manufacture plasticizers for polyvinylchloride.[16] The reaction mechanism of aldol condensation has been well studied as three steps for aldol reaction and one step for condensation of water, leading to the overall reaction expressed as below[17]

$$2C_3H_7CHO \xrightarrow{k} C_7H_{13}CHO + H_2O \quad (1)$$

For an accurate reactor model, it is necessary to obtain intrinsic reaction kinetics under industrially relevent conditions. Applying the pseudo steady-state approximation with

Correspondence concerning this article should be addressed to A. Varma at avarma@purdue.edu.

the first step (enolate formation) as the rate-determining,[18] the kinetics is simplified as first order. Although the reaction at the industrial operating conditions is in the mass transfer controlled regime, the intrinsic reaction kinetic parameters were carefully determined using a stirred cell and the use of penetration theory in our prior work[12]

$$r_{\mathrm{nBAL}}=kC_{\mathrm{nBAL}},\ \left(k=1.712\times10^{8}\mathrm{e}^{-\frac{13.47\pm0.39\ \mathrm{kcal/mol}}{RT}}C_{\mathrm{NaOH}}\right) \quad (2)$$

With these kinetic parameters, the range of the Hatta number for this reaction at the industrial operating conditions is 0.3–1.5, which is in the intermediate reaction regime. In this regime, to develop a reactor model, equations to estimate the interfacial area must also be available. For this purpose, Sauter mean diameter for dispersed-phase droplet is widely used as it can be directly converted to the interfacial area through $a=6\varepsilon_d/d_{32}$. Semiempirial correlations based on the critical Weber number and the isotropic turbulence theory by Kolmogoroff have been developed to obtain the Sauter mean diameter.[19] Typically, correlations composed of the Weber number and the turbulence damping factor are preferred.[20] Although this method is simple and easy to use, the parameters of the correlations have to be determined individually for different cases of reactor geometry and chemical properties.[21]

Experimental measurements of the interfacial area are needed to develop and verify correlations. The chemical method has been used to model a biphasic reactor.[14] In this method, the global interfacial area is obtained from specific chemical reaction systems, such as butylformate or diisobutylene, using the Danckwerts penetration theory in a stirred cell or a stirred tank.[22,23] This method, however, has limitations because it does not directly measure the interfacial area.[24] Also, due to the restriction of this method to $Ha>3$, it cannot be used for the present cases of nBAL aldol condensation at industrial operating conditions where $0.3<Ha<1.5$. As an alternative, the measurement of the interfacial area using a borescope is a direct and *in situ* method.[25] In this technique, actual droplet pictures in a biphasic stirred tank are taken by a CCD camera with a borescope. The drop-size distribution and interfacial area are obtained directly from counting droplets in the pictures.[26] This method, despite labor-intensive droplet counting, is acknowledged to be the most accurate method to obtain the interfacial area.[25,27] Because the aldol reaction is at 80–140°C and temperature can influence the interfacial area, the temperature effect has to be considered. While there are many reports using various methods to determine the interfacial area in a biphasic stirred tank, the relatively high temperature and NaOH concentration (1.14–1.9 M) effects on interfacial area have not been investigated. In this light, the objectives of the present study are:

- Evaluate the effect of temperature and NaOH concentration on interfacial area, based on experiments using a borescope system and modeling using a semiempirical correlation
- Develop a film-based reactor model for the biphasic stirred tank reactor with nBAL aldol condensation
- Determine the effect of the interfacial area modeling on the accuracy of the biphasic reactor model.

Theory

Reactor modeling using the film model

In a biphasic stirred tank reactor for nBAL aldol condensation, the organic phase is composed of nBAL reactant and 2-ethyl-2-hexenal (2EHEL) product, while the NaOH catalyst is in the aqueous phase. The NaOH concentration is considered constant in the aqueous phase with the assumption that the dilution by water as a reaction byproduct can be ignored. nBAL and 2EHEL are slightly soluble and nearly immiscible in the aqueous phase, while NaOH is immiscible in the organic phase. Thus, the reaction occurs in the aqueous phase, shown schematically by the two film theory in Figure 1. The film thickness δ is determined by D/k_{L}. The ultimate goal of the modeling is to estimate the nBAL concentration in the organic phase with time, to indicate reaction progress.

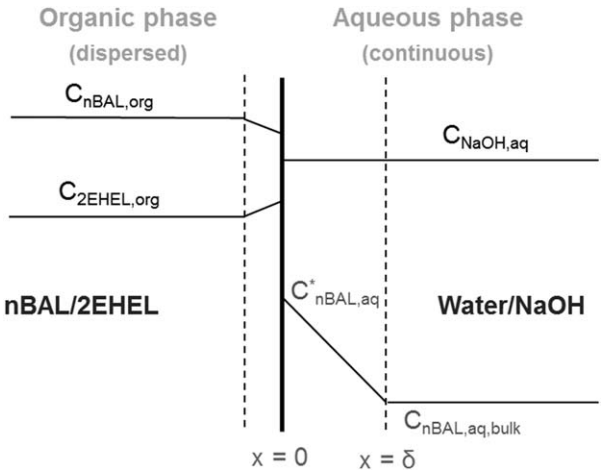

Figure 1. Schematic diagram of the biphasic interface.

As a batch operation, the mass balance of nBAL in the organic phase is described by Eq. 3

$$V_{\mathrm{org}}\frac{dC_{\mathrm{nBAL,org}}}{dt}=-R_{\mathrm{overall}};\ C_{\mathrm{nBAL,org}}=C^{o}_{\mathrm{nBAL,org}}\ \text{at}\ t=0 \quad (3)$$

In the case of intermediate reaction regime, the overall reaction rate of nBAL is determined by mass transfer in the organic film, mass transfer with reaction in the aqueous film and reaction in the bulk aqueous phase.[7] Following the two film resistance theory, the overall reaction rate can be described by the molar flux of nBAL at the interface

$$R_{\mathrm{overall}}=aV_t J_{\mathrm{nBAL}}\big|_{x=0} \quad (4)$$

The film model assumes a stagnant film, which means no change with time. The nBAL aldol condensation has been confirmed as a pseudo-first-order reaction in prior work.[12,18] Thus, the mass balance of nBAL concentration in the film of the aqueous phase is described by Eq. 5

$$D\frac{d^2C_{\mathrm{nBAL,film}}}{dx^2}-kC_{\mathrm{nBAL,film}}=0 \quad \left\{\begin{array}{c} C_{\mathrm{nBAL,film}}=C^{*}_{\mathrm{nBAL,aq}}\ \ at\ x=0 \\ C_{\mathrm{nBAL,film}}=C_{\mathrm{nBAL,bulk}}\ \ at\ x=\delta \\ C^{*}_{\mathrm{nBAL,aq}}=mC^{*}_{\mathrm{nBAL,org}} \end{array}\right\} \quad (5)$$

In the present work, the distribution coefficient, diffusivity, and mass-transfer coefficient for the continuous (aqueous) phase, including viscosity, and density variations, were obtained from our previous study.[12] From the solution of Eq. 5, the nBAL concentration in the aqueous film is

$$\begin{aligned} C_{\mathrm{nBAL,film}}=\ & C^{*}_{\mathrm{nBAL,aq}}\cosh\sqrt{\frac{k}{D}}x+\frac{1}{\sinh Ha} \\ & \left(C_{\mathrm{nBAL,bulk}}-C^{*}_{\mathrm{nBAL,aq}}\cosh Ha\right)\sinh\sqrt{\frac{k}{D}}x \end{aligned} \quad (6)$$

which is valid for $0\ \le x\le\delta$. The molar flux of nBAL in the film is given by

$$J_{\mathrm{nBAL}}=-D\left(\frac{dC_{\mathrm{nBAL,film}}}{dx}\right)=\frac{k_L Ha}{\sinh Ha}\left(C^{*}_{\mathrm{nBAL,aq}}\cosh\left(Ha-\sqrt{\frac{k}{D}}x\right)-C_{\mathrm{nBAL,bulk}}\cosh\sqrt{\frac{k}{D}}x\right) \tag{7}$$

To obtain $C_{\mathrm{nBAL,bulk}}$, the mass balance of C_{nBAL} in the bulk region of the aqueous phase is described by Eq. 8

$$\varepsilon_{\mathrm{bulk}}V_t\frac{dC_{\mathrm{nBAL,bulk}}}{dt}=aV_tJ_{\mathrm{nBAL}}|_{x=\delta}-\varepsilon_{\mathrm{bulk}}V_tkC_{\mathrm{nBAL,bulk}} \quad \left\{\begin{array}{c} C_{\mathrm{nBAL,bulk}}=0 \text{ at } t=0 \\ \varepsilon_{\mathrm{bulk}}=\varepsilon_{\mathrm{aq}}-a\delta \end{array}\right\} \tag{8}$$

From Eqs. 7 and 8, we have

$$C_{\mathrm{nBAL,bulk}}=\frac{\alpha_1}{\alpha_2}(1-e^{-\alpha_2 t})\approx\frac{\alpha_1}{\alpha_2}\ (kt\gg 1) \tag{9}$$

where $\alpha_1=\frac{a\ Ha\ k_L}{\varepsilon_{\mathrm{bulk}}\sinh\ Ha}C^{*}_{\mathrm{nBAL,aq}}$, $\alpha_2=\frac{a\ Ha\ k_L}{\varepsilon_{\mathrm{bulk}}\tanh\ Ha}+k$

The assumption of Eq. 9 ($kt\gg 1$) is satisfied within 1 s in the actual calculations for nBAL aldol condensation under the reaction conditions. Therefore, with Eqs. 7 and 9, R_{aq} is given by

$$R_{\mathrm{overall}}=aV_tJ_{\mathrm{nBAL}}|_{x=0}=aV_t\ mC^{*}_{\mathrm{nBAL,org}}\ k_L\left(1-\frac{1}{\cosh^2 Ha+\alpha_3 k}\right)\frac{Ha}{\tanh Ha} \tag{10}$$

where $\alpha_3=\frac{\varepsilon_{\mathrm{bulk}}\sinh Ha\cosh Ha}{a\ Ha\ k_L}$

The mass-transfer rate in the organic phase film is simply described by Eq. 11, because no reaction occurs in the organic phase. The mass-transfer coefficient for the organic phase as the dispersed phase is presented in Appendix A

$$R_{\mathrm{overall}}=aV_tk_{\mathrm{L,org}}(C_{\mathrm{nBAL,org}}-C^{*}_{\mathrm{nBAL,org}}) \tag{11}$$

Eliminating $C^{*}_{\mathrm{nBAL,org}}$ from Eqs. 10 and 11, the overall reaction rate is rearranged as a function of the nBAL concentration in the bulk organic phase and the operating conditions of temperature, NaOH concentration and the agitation power, as shown in Eq. 12

$$R_{\mathrm{overall}}=k'_{\mathrm{overall}}C_{\mathrm{nBAL,org}} \tag{12}$$

where

$$\left\{\frac{1}{k'_{\mathrm{overall}}}=\frac{1}{aV_t\ m\ k_L\left(1-\frac{1}{\cosh^2 Ha+\alpha_3 k}\right)\frac{Ha}{\tanh Ha}}+\frac{1}{aV_tk_{\mathrm{L,org}}}\right\} \tag{13}$$

In fact, we can view the two terms on the r.h.s. of Eq. 13 as the resistances corresponding to the aqueous and organic phases, respectively to yield

$$\frac{1}{R_{\mathrm{overall}}}=\frac{1}{R_{\mathrm{aq}}}+\frac{1}{R_{\mathrm{org}}} \tag{14}$$

which is the typical way to note that the overall resistance equals the sum of the resistances in series.

Substituting Eq. 12 in Eq. 3, the latter becomes a simple first-order linear ordinary differential equation for the nBAL concentration in the organic phase, which has the solution

$$\ln\ C_{\mathrm{nBAL,org}}=-\frac{k'_{\mathrm{overall}}}{V_{\mathrm{org}}}t+\ln\ C^{\mathrm{o}}_{\mathrm{nBAL,org}}=\ -k_{\mathrm{overall}}t+\ln\ C^{\mathrm{o}}_{\mathrm{nBAL,org}} \tag{15}$$

Using Eq. 15, it is possible to determine the change of nBAL concentration in the organic phase, with time. However, this evaluation still requires information for the interfacial area a as a function of agitation power, reactor geometry, and hydrodynamic properties including density, viscosity, and interfacial tension.

Interfacial area estimation

The dispersed phase in a biphasic stirred tank is composed of several different sized droplets. The Sauter mean diameter, obtained from the number of droplets (n_i) with diameter (d_i), is useful to determine the interfacial area, representing the droplet distribution of the dispersed phase. The Sauter mean diameter is defined as

$$d_{32}=\frac{6\varepsilon_d}{a}=\frac{\sum_i n_i d_i^3}{\sum_i n_i d_i^2} \tag{16}$$

If the biphasic system is in turbulence so that drop diameters are much larger than Kolmogoroff's length scale and the drop is inviscid, by combining the critical Weber number for breakup of droplets by Hinze[28] and Kolmogoroff's theory of isotropic turbulence,[29] the maximum drop diameter ($d_{\max}$) is described by Eq. 17[20]

$$\frac{d_{\max}}{d_{\mathrm{imp}}}=\ C_1We^{-0.6} \tag{17}$$

The maximum diameter is substituted with the Sauter mean diameter following several reports that they are linearly proportional[20,30]_ENREF_30, although some researchers[19,31] disagree. Doulah[32] extended this equation to consider that the Sauter mean diameter increases with the holdup of the dispersed phase due to the coalescence and damping of turbulence

$$\frac{d_{32}}{d_{\mathrm{imp}}}=\ C_1(1+C_2\varepsilon_{\mathrm{org}})We^{-0.6} \tag{18}$$

C_1 is an empirical parameter which includes the effects of reactor geometry, power number, and several proportional factors, while C_2 represents the turbulence damping or coalescence factor. The reported ranges of C_1 and C_2 values are 0.04–0.4 and 2–10, respectively.[33] Equation 18 is the most frequently used form to estimate the Sauter mean diameter. Further, a viscosity factor has also been introduced to include the effect of different chemical systems, as described by Eq. 19[34,35]

$$\frac{d_{32}}{d_{\mathrm{imp}}}=\ C_1(1+C_2\varepsilon_{\mathrm{org}})We^{-0.6}\left(\frac{\mu_d}{\mu_c}\right)^{C_3} \tag{19}$$

C_3 is an exponent for the viscosity factor, which has reported values up to 0.44 for different chemical systems.[35] Models for the interfacial tension used in this study are described in Appendix B.

Interfacial Area

The interfacial area in the biphasic stirred tank reactor for nBAL aldol condensation was evaluated through the droplet pictures taken using a borescope system. A new

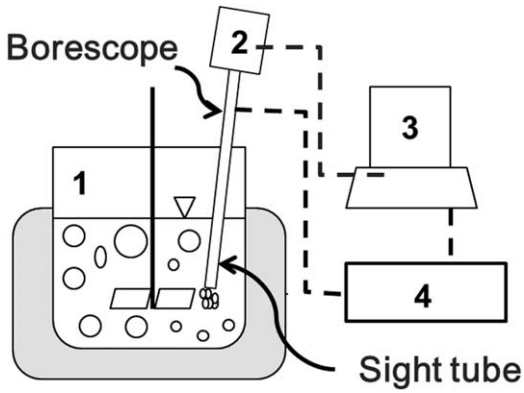

Figure 2. Schematic diagram of the biphasic stirred tank with the borescope system; 1–stirred tank, 2–CCD camera, 3–Personal computer, 4–fiber optic strobe.

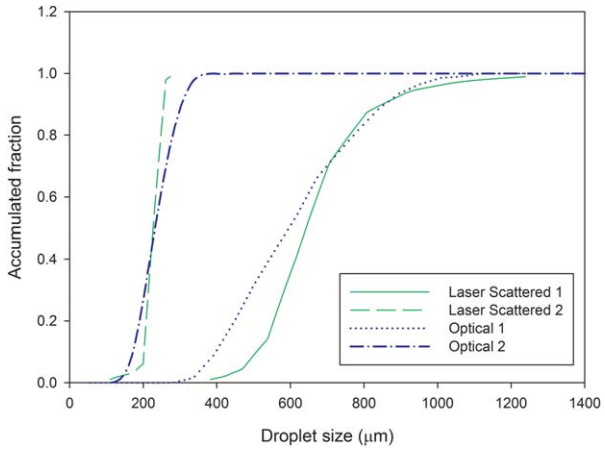

Figure 3. The calibration of the borescope system with glass beads (1: 250 μm glass beads, 2: 20–30 mesh glass beads).

[Color figure can be viewed in the online issue, which is available at wileyonlinelibrary.com.]

correlation for the interfacial area was developed after assessing the predictions of literature correlations in comparison with the experimental measurements from this work.

Experimental apparatus

The measurements of the interfacial area were conducted in a 300 mL stainless steel reactor, with height to diameter ratio 1.6. A four blade and 45°-pitched paddle was used to agitate the biphasic solution. The diameter ratio of the impeller to the reactor was 0.5. The visualization system installed in the reactor consisted of a borescope with a sight tube, a CCD camera, a fiber optic strobe and a personal computer as shown in Figure 2. The borescope had a small diameter ($\varnothing = 2.4$ mm; Gradient Lens Corporation Pro Superslim) to prevent the disruption of drop-size distribution when installed in the reactor. The sight tube, using a 1/8″ or 3/16″ stainless tube and a borosilicate sight glass, was used to protect the borescope and help to focus the image. A two million pixel CCD camera (Sony XCDU100) and a fiber optic strobe (Excelitas X-1500) were used to take pictures of droplets which were sent to the personal computer for storage.

Calibration

Although the borescope system provided the pictures of actual droplets, the focus distance between the lens of the borescope and the actual droplets required calibration of the system. For this, two sets of glass beads were used (20–30 mesh and 250 μm). For reference, the particle-size distribution was measured by a laser scattering particle size analyzer as the standard (HORIBA LA-950). The particle-size distributions, suspended under water, were then measured by manually counting 200–400 glass beads in many pictures obtained using the borescope system. The results from the two different methods were compared, as shown in Figure 3, where it may be seen that the particle size distributions from the borescope were somewhat broader than the actual size. This may be caused by counting particles which are slightly out of focus and appear smaller when they are far away from the sight glass. Despite this limitation,[26,36] the borescope system provides a good estimate of the particle size distribution, hence is suitable for use in the current study.

Experimental procedure

To measure the droplet size distribution, unreactive 2EHEL (2-ethylhexenal) was selected as the organic phase because nBAL reacts in the aqueous NaOH solution under the experimental conditions. After each experiment, gas chromatography (GC) analysis conducted after taking pictures confirmed that 2EHEL did not react in the NaOH solution. In fact, 2EHEL was prepared by aldol condensation of nBAL and stored in a glass jar (2EHEL purity $> 95\%$). For the droplet size experiments, a mixture of 140 mL NaOH solution and 60 mL 2EHEL was placed in the reactor, pressurized with nitrogen up to 1.5 barg to prevent azeotropic boiling. After a minimum of 10 min. for each experimental condition, 20–40 pictures of droplets were taken, with most drops appearing perfect spheres as shown in Figure 4. The pictures were taken from the top and bottom positions of the reactor to obtain average values for the entire vessel. A minimum of 200 drops for each position, totaling 400 drops, were counted for each experimental condition. In general, high rpm produced smaller droplets and their size at the top position was somewhat larger than at the bottom, as shown in Figure 5. This may be caused by droplet breakup near the agitator and coalescence at the stator zone far from the agitator, which conforms to literature reports for biphasic stirred tanks.[37] The possible disturbing effect of the borescope was checked by computational fluid dynamics (CFD) technique, as described in Appendix C. Because the borescope caused less than 1% difference in the P/V (power per volume) of the reactor, it was shown that the effect was negligible. Thus, the preliminary tests demonstrated that the borescope system was well suited for the droplet-size distribution study to provide the interfacial area.

Measurements of the Sauter mean diameters

The Sauter mean diameters (d_{32}) were measured in the range 25–110°C, 0–1.9 M C_{NaOH}, and 600–1000 rpm. The borescope system allowed measurements of the drop diameters below 110°C while most prior studies reported in the literature were conducted near 25°C. Unfortunately, due to the upper temperature limit of the borescope, it was not possible to measure droplets in the higher 120–140°C region of the

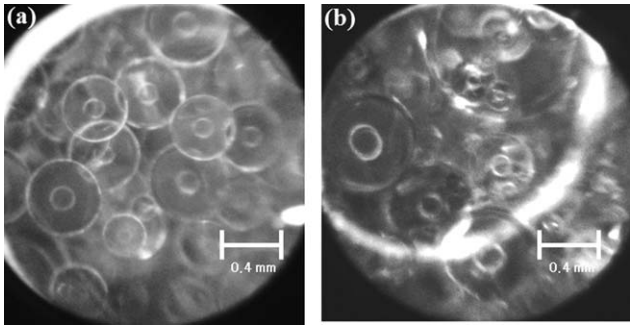

Figure 4. Drop pictures by the borescope system; a) 110°C, 1.9 M C_{NaOH}, 800 rpm; b) 25°C, 0 M C_{NaOH}, 600 rpm.

industrial operating condition. For all experiments, the ratio of the dispersed phase was maintained at 0.3, similar to the experimental conditions during reaction. As shown in Figure 6, all three variables of rpm, temperature and NaOH concentration influence d_{32} measurements. As expected, the effect of agitation power (rpm) was much larger than the others. Interestingly, however, the effects of temperature and C_{NaOH} were also significant. The Sauter mean diameters of 2EHEL in NaOH solution increased with temperature increase and decreased with C_{NaOH} increase. The physical properties including viscosity, density, and interfacial tension are affected by temperature and NaOH concentration, which consequently influence Sauter mean diameters. With temperature increase, the viscosity correction term discussed in the theory section increases, although viscosities for both the dispersed phase and the continuous phase decrease. This is because the viscosity for the continuous phase, using the correlation from Laliberte,[38] decreases more significantly than for the dispersed phase due to the effect of temperature as shown in Table 1. The increased viscosity correction term results in larger d_{32}. Regarding the Weber number term only, since the interfacial tension from Appendix B decreases slightly with temperature increase, the Sauter mean diameter should decrease slightly as well. However, the experimental result is the opposite (Figure 6c). This implies that with respect to the temperature change, the effect of the viscosity correction term is larger than that of the interfacial tension. Concerning the effect of increasing NaOH concentration, the viscosity of the continuous phase increases and results in smaller drops while the interfacial tension slightly increases and results in larger drops, as shown in Table 2. Because the observed d_{32} decreases with increasing NaOH concentration (Figure 6c), d_{32} is affected more by the viscosity correction, rather than the interfacial tension, similar to the effect of temperature. Thus, the viscosity correction term is necessary to explain the effects of temperature and NaOH, and cannot be ignored.

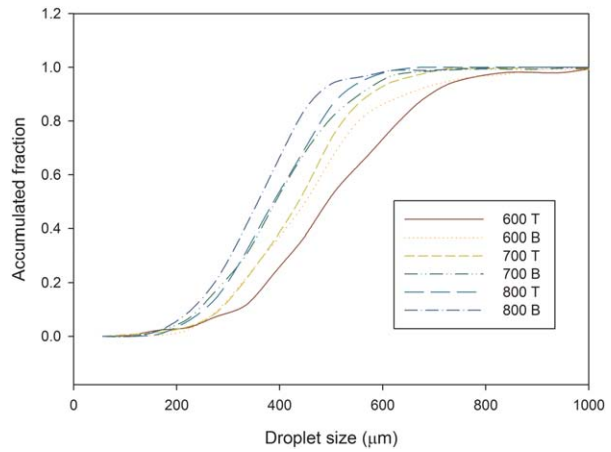

Figure 5. Accumulated droplet size distributions at 110°C, 1.9 M C_{NaOH}; T-top, B-bottom; the numbers in the legend denote agitator rpm.

[Color figure can be viewed in the online issue, which is available at wileyonlinelibrary.com.]

Estimation of the Sauter mean diameter using correlations

To develop an accurate reactor model, it is necessary to build an estimation model for the Sauter mean diameter. In this study, with $3 - 7 \times 10^4$ impeller Reynolds number, the biphasic system was in turbulence. In addition, the measured d_{32} was much larger than the Kolmogoroff's length scale η=20–50μm, calculated with the averaged turbulent dissipation rate. Further, with 0.3–1.1 cP μ_d, drops in this system may be regarded as inviscid. Under these conditions, there are several available correlations obtained from measurements with various chemical systems, measurement methods and operating conditions. Among these, correlations with 0.3 or similar fraction of the dispersed phase were selected[20,23,33–35,39–42] and evaluated with the measurement data of this study as shown in Figure 7 and Table 3. Remarkably, the role of the viscosity correction term was important based on the R^2 values from correlations with and without the viscosity correction term, which were ~60% and 30–36%, respectively, as discussed in the previous section. However, because even ~60% R^2 is not enough accuracy, and particularly to account for the effects of temperature and NaOH, a new correlation based on Eq. 19 was developed by fitting with the measurements of this study (Figure 6)

$$d_{32}/d_{\mathrm{imp}} = 0.207 * We^{-0.53} \left(\frac{\mu_{\mathrm{d}}}{\mu_{\mathrm{c}}}\right)^{0.94} \tag{20}$$

The exponent of the Weber number for the full dataset was −0.53, which is slightly larger than −0.6 and may arise in relatively larger dispersed-phase fraction systems due to the complex breakage mechanism, as studied by Desnoyer et al.[42] The exponent of the viscosity correction term was 0.94, which is larger than 0.25–0.44 in prior studies[34,35] where the correction term was used solely for different chemical species.

Equation 20 was compared with prior works by Godfrey et al.[35] and Santiago and Trambouze,[39] which are representative of correlations with and without the viscosity correction term, respectively, as shown in Figure 8. The latter did not follow the trend with the temperature and NaOH concentration because it did not include a viscosity correction term, while the former showed a relatively better result owing to its viscosity correction term. The correlation developed in this work (Eq. 20) showed the best fit with the experimental data obtained from various temperatures and NaOH concentrations. The R^2 of this correlation was 89.5%, sufficiently accurate for the reactor modeling, as compared to 31–62% R^2 for the other correlations shown in Table 3. As shown in Figure 7, Eq. 20 is accurate within ±15% range and may be used for modeling the biphasic stirred tank reactor for nBAL aldol condensation.

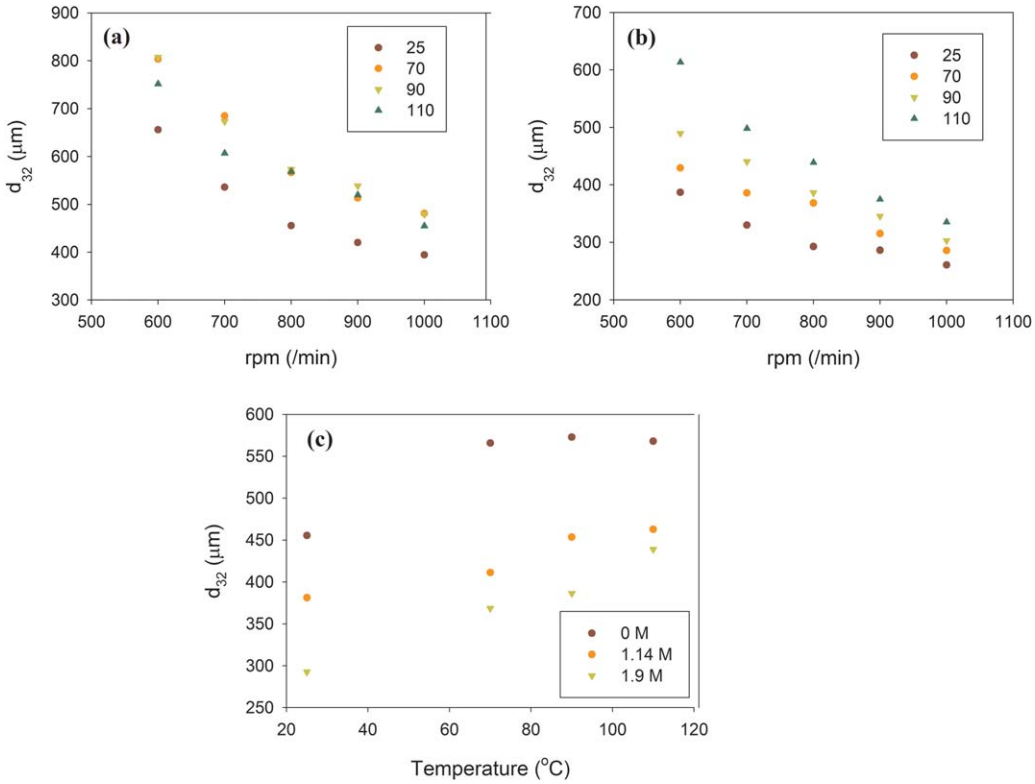

Figure 6. d_{32} measurements of 2EHEL (30%) / Water (70%) system at 25–110°C, 0–1.9 M C_{NaOH}, 600–1000 rpm; (a) 0 M C_{NaOH}, 25–110°C, (b) 1.9 M C_{NaOH}, 25–110°C, (c) 800 rpm, 0–1.9 M C_{NaOH}.

[Color figure can be viewed in the online issue, which is available at wileyonlinelibrary.com.]

Biphasic Stirred Tank Reactor for nBAL Aldol Condensation

With the interfacial area investigated in the previous section, the biphasic stirred tank reactor for nBAL aldol condensation was studied both by experiments and modeling. The effect of the interfacial area estimation on predictions of the overall reactor model was evaluated.

Experimental setup

The reaction experiments were carried out in a 300 mL stirred tank reactor system, shown in Figure 9. The reactor, including the agitator, was the same used in the previous section. The reactor had a thermocouple, a heating jacket for external heating and a cooling coil inside the reactor to control the reaction temperature. The injector was used to preheat nBAL before the reaction and to inject nBAL into the reactor through a nozzle to initiate the reaction. Heating tape with a temperature controller was used for preheating the injector, while pressurized nitrogen was used for injection and initial venting. To stabilize the drop distribution of the organic phase as rapidly as possible, the injection nozzle was located near the agitator and modified to create a spray when nBAL was injected. For sampling, 1/8″ OD stainless steel tube and 1/16″ OD copper tube were used inside the reactor vessel and for the condenser, respectively. The copper tube was dipped inside an ice water bath condenser, to quench the samples. The total volume of sampling tubes was about 0.08 mL, which was about 4% of a 2 mL sample volume.

The organic phase samples were analyzed by GC (HP 5890 II) equipped with an Agilent DB-WAXetr capillary column (50 m × 0.32 mm) and flame ionization detector under the following conditions: helium as carrier gas (2.6 mL/min), inlet and detector temperatures 250°C, oven temperature from 80 to 220°C and injection volume 0.5 μL with split. Acetonitrile (Sigma-Aldrich, > 99.9%) was selected as the internal standard. Normal-butyraldehyde (nBAL, Sigma-Aldrich, > 99%) and 2-ethyl-2-hexenal (2EHEL, Sigma-Aldrich, > 93%) were used for calibration of the GC. The R^2 values of all GC calibrations were 99.6%.

The experiments started with preparation of NaOH solution. The NaOH solution (50% in water, Sigma-Aldrich) was diluted with deionized water to obtain specific concentrations, which were confirmed by pH meter (OMEGA PHB-209). The ratio of nBAL to NaOH solution was 0.3, similar to the industrial operating condition. 140 mL of NaOH solution and 60 mL of nBAL were prepared in the reactor vessel

Table 1. Temperature-Dependent Viscosities and Interfacial Tension for the Dispersed and Continuous Phases at 1.9 M C_{NaOH}

T (°C)	μ_d	μ_c	μ_d/μ_c	σ
25	1.06	1.31	0.80	23.5
70	0.65	0.56	1.16	21.7
90	0.55	0.43	1.27	20.8
110	0.47	0.35	1.35	19.8

Table 2. Viscosities and Interfacial Tension for Dispersed and the Continuous Phases at 70°C

C_{NaOH}	μ_d	μ_c	μ_d/μ_c	σ
0	0.65	0.40	1.61	20.6
1.14	0.65	0.47	1.39	21.3
1.9	0.65	0.56	1.16	21.7

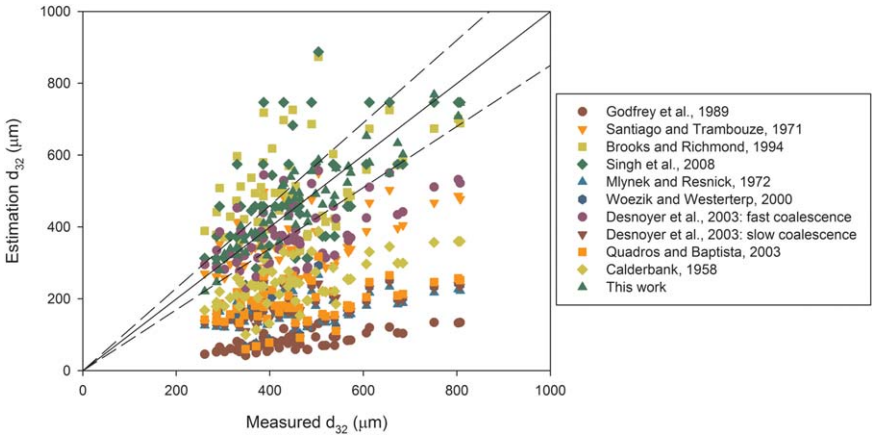

Figure 7. Parity plot for the Sauter mean diameters estimated by published correlations; the dash lines represent ±15% errors.

[Color figure can be viewed in the online issue, which is available at wileyonlinelibrary.com.]

and injector, respectively. After preheating both to the target temperature, nBAL was injected into the reactor in less than 2 s by 200 psig Nitrogen. The reactor was operated at 140–200 psig pressure to prevent azeotropic boiling between nBAL and water during injection of nBAL and initiation of the reaction. The reactor temperature was controlled within ± 2°C by a PID controller. Four liquid samples were taken after 10 or 20 s at 10 s intervals. The removed samples were stabilized for 0.5–1 min to separate the organic and aqueous phases. The separated organic phase was collected using a 3 mL disposable syringe, and analyzed by GC. The repeatability error for each concentration point was less than 5%. The mass balance was checked after each experiment and the error was always less than 1%.

Preliminary studies

The solubilities of nBAL and 2EHEL in the NaOH solution may change when samples are transferred from the reactor at high temperature to a stabilized condition at room temperature. To evaluate this effect, the error between the two conditions was calculated with the UNIQUAC activity model.[43] The predicted error between them was less than 3.3% for the organic phase fraction 0.3, indicating that the effect was negligible.

From Eq. 12, the overall reaction order of nBAL should be first order, as described in the Theory section. This was confirmed by the linear relation of ln $C_{nBAL,org}$ with time according to Eq. 15 for a range of conditions, as shown in Figure 10.

As noted previously, the industrial operating temperature for this reaction is 80–140°C.[16] In our prior study, the intrinsic kinetics were obtained over 110–150°C due to Hatta number restrictions.[12] Therefore, two design of experiment (DOEs) were prepared to verify the biphasic reactor model, as described by Eq. 12. One (DOE 1) was designed by the inscribed central composite method[44] over 80–140°C, 0.05–2.0 M C_{NaOH}, and 600–1000 rpm to cover the full industrial operation range. The range of the other (DOE 2) was 110–130°C, 0.76–1.52 M C_{NaOH}, and 700–900 rpm, selected as being in the narrow kinetic experimental range using the Box-Behnken design.[44] DOE 1 and 2 were composed of 20 and 15 cases, including six and three repeats of the central points, respectively.

Experimental results and evaluation of the reactor model

Experiments for the two DOE sets were carried out in the 300 mL stirred tank reactor. Both sets were confirmed as statistically reliable using MINITAB with 2.8% and 3.4% repeatability error for the central points of DOE 1 and 2, respectively. The experiments where the total conversion ranges were less than 20% were excluded. These cases, when the reaction rate is too fast or too slow for the operating conditions of temperature, C_{NaOH} or rpm, can lead to large experimental errors because the extracted data from experiments is the slope of concentrations from successive samples. Following this criterion, 27 points were used to evaluate the model, while eight points were excluded. Most of the excluded points were obtained at greater than 80% nBAL conversion (below 2 M of C_{nBAL} at 10 s) under high temperature and high rpm. The overall reaction constants ($k_{overall}$) were obtained from C_{nBAL} values of each experiment by Eq. 15 and used to verify the $k_{overall}$ values

Table 3. Summary of the Correlations Used in Figure 7

Reference	Measurement Method	Dispersed Phase Hold Up, ε_{org}	d_{32} (mm)	N (s^{-1})	R^2 (%)
Godfrey et al., 1989	Photography	0.1–0.5	0–0.3	7–9	61.7
Calderbank, 1958	Light transmittance	0–0.2	0.05–0.32		57.0
Santiago and Trambouze, 1971	Chemical			15–30	31.7
Quadros and Baptista, 2003	Chemical	0.061–0.166	0.01–0.2	5–25	31.9
Woezik and Westerterp, 2000	Chemical	0–0.3	0.03–0.15	15–25	31.9
Brooks and Richmond, 1994	Photography	0.1–0.5	0–0.4		31.7
Singh et al., 2008	Photography (offline)	0.2–0.5	0.4	1.7–2.5	36.1
Mlynek and Resnick, 1972	Photography (*In situ*)	0.025–0.34	0.14–0.46	2.3–8.3	31.9
Desnoyer et al., 2003; slow coalescence	Laser granulometer	0.1–0.6	0.15–0.35	10.2–15	31.9

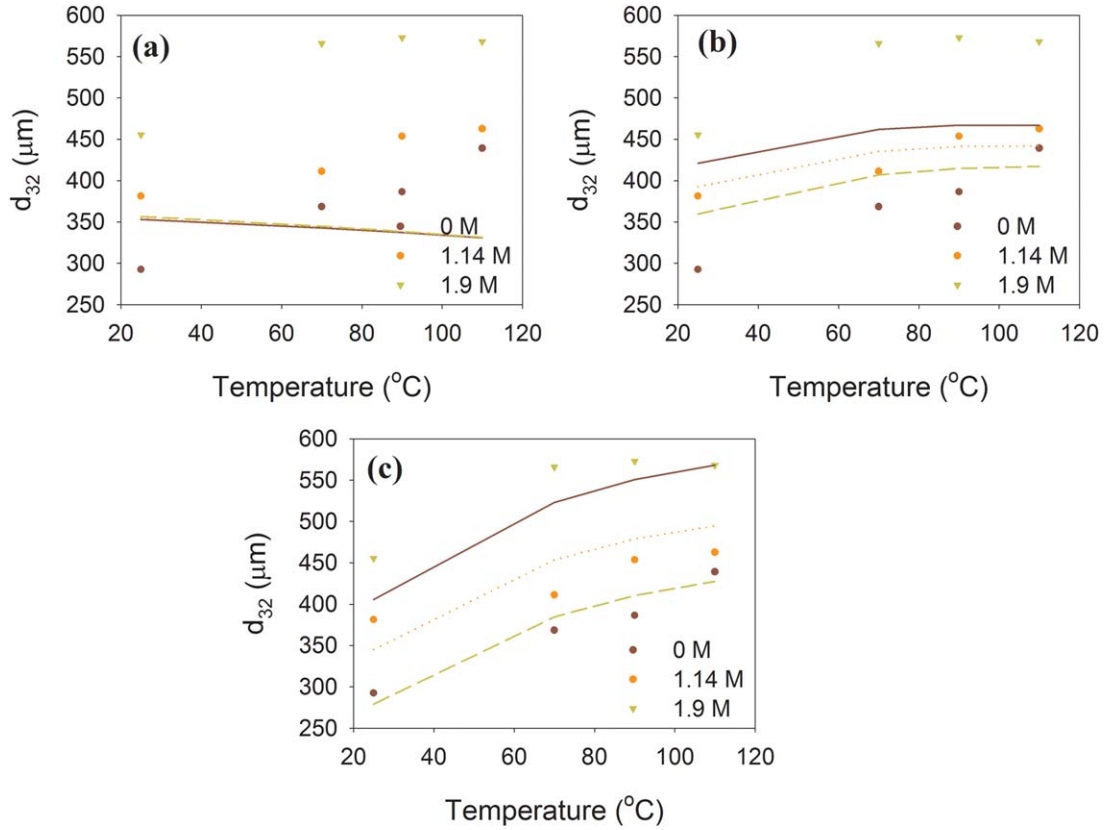

Figure 8. Comparison between the measurements (points) and the estimation (line) by (a) Santiago and Trambouze (1971); (b) adjusted Godfrey et al. (1989); (c) this work.

[Color figure can be viewed in the online issue, which is available at wileyonlinelibrary.com.]

estimated from Eq. 13. The average differences in overall reaction rates between the experimental and predicted values were 10% and 4%, for DOE 1 and 2, respectively. All estimations for DOE 1 and 2 were in ±15% error range as shown in Figure 11a. The average estimation error for DOE 2 was lower than that for DOE 1 because DOE 2 is within the experimental conditions for the intrinsic reaction kinetics in our prior work.[12] The results of DOE1 demonstrate that the intrinsic kinetics from 110–150°C can be extrapolated down to 80°C and also that the film model, combining the intrinsic kinetics from the stirred cell and the interfacial area correlation from the borescope system without any adjustable parameters, is applicable for the entire industrial operating range.

To evaluate the effect of the interfacial area estimation on the accuracy of the reactor model, the predicted results were

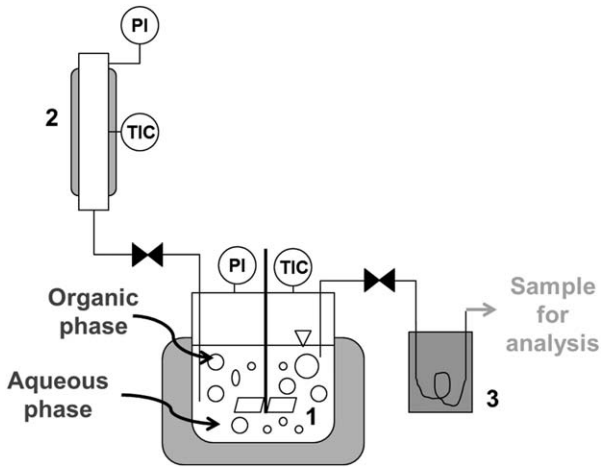

Figure 9. Schematic diagram of the biphasic stirred tank for nBAL aldol condensation. (1: stirred tank reactor, 2: injector, 3: condenser, PI: pressure indicator, TIC: temperature indicator / controller.)

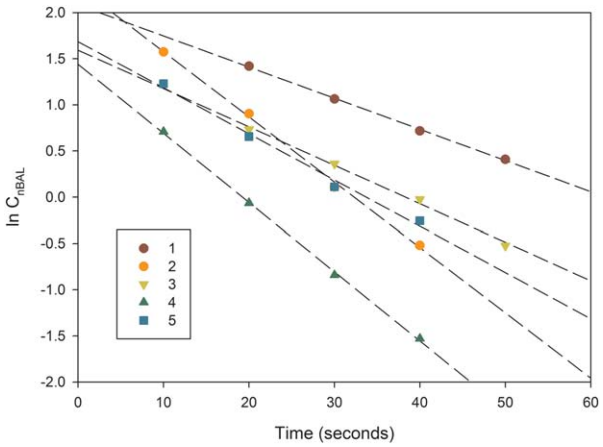

Figure 10. Confirmation of first-order reaction through ln C_{nBAL} as a function of time. 1: 110°C, 1.03 M C_{NaOH}, 600 rpm; 2: 110°C, 1.03 M C_{NaOH}, 800 rpm; 3: 120°C, 1.52 M C_{NaOH}, 700 rpm; 4: 120°C, 0.76 M C_{NaOH}, 900 rpm; 5: 92°C, 1.60 M C_{NaOH}, 919 rpm

[Color figure can be viewed in the online issue, which is available at wileyonlinelibrary.com.]

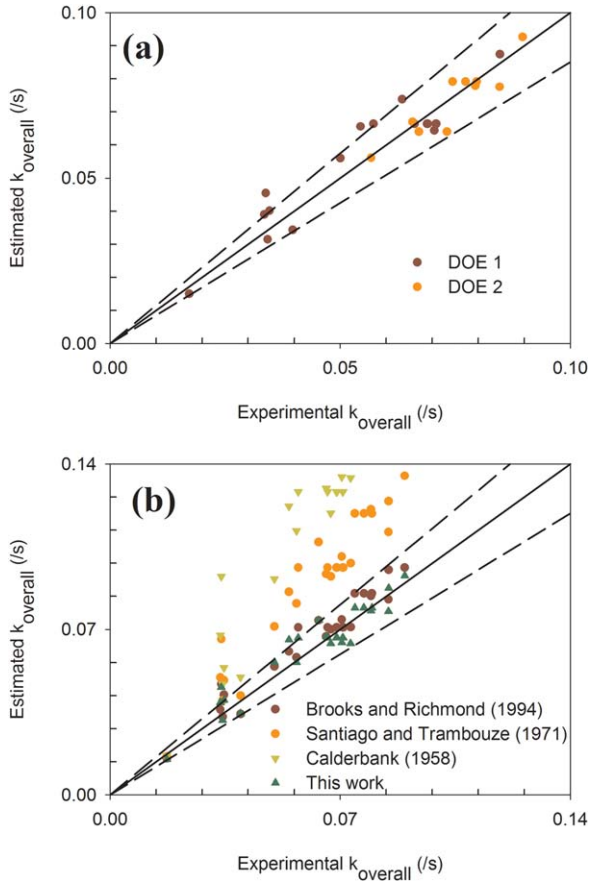

Figure 11. Parity plots of the overall rate constant—the experiments vs. the estimations by the model using (a) the correlation developed in this work; (b) the correlations from literature; the dash lines represent ±15% errors.

[Color figure can be viewed in the online issue, which is available at wileyonlinelibrary.com.]

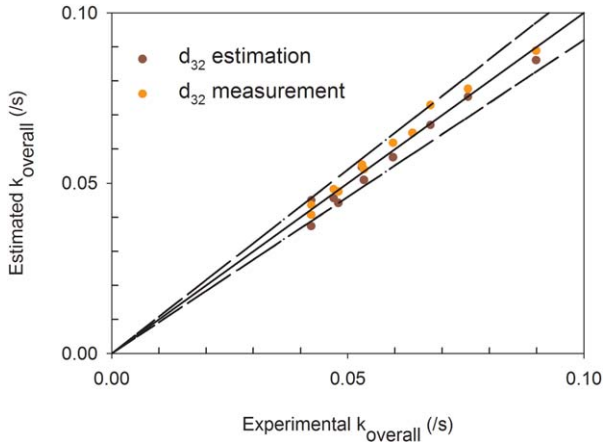

Figure 12. Comparison of the estimation accuracy between the model using d_{32} estimations and d_{32} measurements; the dash lines represent ±8% errors.

[Color figure can be viewed in the online issue, which is available at wileyonlinelibrary.com.]

compared with estimations from different literature interfacial area correlations, using the same reactor model, as shown in Figure 11b. It may be seen that the interfacial area correlation has a significant impact on the estimation accuracy of the reactor model. It is seen once again that the interfacial area correlation developed in this work (Eq. 20) is more appropriate to describe reactor performance than prior correlations available in the literature.

Although the developed interfacial area correlation was optimized for the biphasic nBAL aldol condensation in the industrial operating range, the estimation error of interfacial areas was around ±15%, as described in the Interfacial Area section. Since the estimation error of the interfacial area directly affects the accuracy of the reaction rate estimation, the reaction rate predictions should be better with the reactor model combined with d_{32} measurement data directly from the borescope system, not through the correlation. To confirm this, 11 additional reaction experiments were conducted under the same operating conditions along with 11 interfacial area measurements obtained with no reaction (see Experimental Procedure of Interfacial Area section). The range of the experiments was 90–110°C, 1.14–1.9 M C_{NaOH}, and 600–1000 rpm. As shown in Figure 12, the estimation error of the reactor model using the direct d_{32} measurements was within ±8%, which is significantly lower than the ±15% error range for DOE 1 and 2, as shown in Figure 11a, when the developed correlation was used. The predictions of the model using the correlation were compared with estimations of the reactor model using d_{32} measurements, as shown in Table 4 where R^2 values were 97.3% and 98.5%, respectively. Alternatively, these can be expressed as 2.7% and 1.5% R^2 errors, respectively. The standard deviation of the rate prediction errors was 5.0% and 3.3% for reactor models with d_{32} estimations and d_{32} measurements, respectively. From both evaluations, it is apparent that the errors of the reactor model predictions using d_{32} estimations were nearly double those using d_{32} measurements. This shows that the effect of the d_{32} estimation error is significant on the biphasic reactor model for nBAL aldol condensation, suggesting that the modeling accuracy may be improved with more effective d_{32} estimations.

Concluding Remarks

Experimental and modeling studies of nBAL aldol condensation in a 300 mL biphasic stirred tank were conducted to estimate the overall reaction rate under industrial operating conditions in the intermediate reaction regime, accounting for the interfacial area, mass transfer in both phases, as well as the intrinsic reaction kinetics.

Table 4. $k_{overall}$ from Experiments, the Models Using d_{32} Estimations and d_{32} Measurements

			$k_{overall}$ (s^{-1})		
Temp °C	C_{NaOH} M	RPM min^{-1}	Experiment	d_{32} estimation	d_{32} measurement
110	1.90	800	0.064	0.065	0.065
110	1.90	900	0.075	0.075	0.078
110	1.90	1000	0.090	0.086	0.089
110	1.90	700	0.053	0.055	0.055
110	1.90	600	0.042	0.045	0.043
110	1.14	800	0.068	0.067	0.073
90	1.14	800	0.047	0.046	0.048
90	1.90	800	0.048	0.044	0.047
90	1.90	1000	0.060	0.058	0.062
90	1.90	700	0.042	0.037	0.041
90	1.90	900	0.053	0.051	0.054

The interfacial area for reactor modeling was obtained using the experimental measurements and semiempirical correlation for the Sauter mean diameter. The borescope system as a physical and *in situ* measurement technique was used to obtain the data under 25–110°C, 0–1.9 M C_{NaOH}, and 600–1000 rpm at 0.3 of the organic phase ratio. The measurements showed that the effects of temperature and C_{NaOH} on the interfacial area were significant in the biphasic system of 2EHEL and NaOH solution. To consider these, the semiempirical correlation was modified with a viscosity correction term and its empirical parameters were determined using the measurement data. The predictions of the developed correlation were significantly better than those of other correlations available in the literature.

The biphasic reactor model was developed based on interfacial area and the intrinsic reaction kinetics. The model was successfully verified with the reaction experimental results through two different DOE sets at 80–140°C, 0.05–2.0 M C_{NaOH}, and 600–1000 rpm. The comparison of the experimental results with the biphasic reactor model predictions directly using the interfacial area measurements showed that the model accuracy was significantly improved.

This study shows that the film model, considering film resistance in the organic phase and reactions in both the aqueous film and the bulk region of the aqueous phase, successfully estimates the biphasic stirred tank reactor performance for nBAL aldol condensation in the intermediate reaction regime. This work is expected to be helpful for design and optimization of biphasic reactors for other applications.

Acknowledgments

We thank Mr. Zhiyang Yu for some experiments. This work was supported by the Hanwha Chemical Company (student fellowship for Shinbeom Lee) and the R. Games Slayter discretionary fund. This contribution was identified by Sagar Sarsani (SABIC) as the Best Presentation in the session "Multiphase Reaction Engineering II" of the 2014 AIChE Annual Meeting in Atlanta, GA.

Notation

a = effective interfacial area, m^2/m^3
$C, C_i, C_{i,j}$ = molar concentration of component i in phase j or region, $kmol/m^3$
C_D = drag coefficient (1 for cube, 0.47 for sphere)
C_i^o, $C_{i,j}^o$ = initial molar concentration of component i in phase j at $t=0$, $kmol/m^3$
D = diffusivity of nBAL into the aqueous phase, m^2/s
$D_{i,j}$ = diffusivity of component i in phase j, m^2/s
d, d_i = drop diameter, m
d_{10} = mean diameter, m, $\frac{\sum_i n_i d_i}{\sum_i n_i}$
d_{32} = Sauter mean diameter, m, $\frac{\sum_i n_i d_i^3}{\sum_i n_i d_i^2}$
d_{imp} = Impeller diameter, m
g = the acceleration of gravity, m/s^2
J_i = molar flux of component i , $kmol/m^2.s$
k = reaction rate constant, s^{-1}
k_L = mass-transfer coefficient of aqueous phase, m/s
$k_{L,i}$ = mass-transfer coefficient of phase i, m/s
$k_{overall}$ = overall reaction rate constant, s^{-1} , $k_{overall} = V_{org} k_{overall}$
$k_{overall}$ = overall reaction rate constant, m^3/s,
m = distribution coefficient of nBAL between organic phase and NaOH solution
n = agitation speed, /s
n_i = number of droplets
P = agitation power, J/s
$R_{overall}$ = overall reaction rate, kmol/s
R_i = resistance of Intrinsic reaction rate of component i, $kmol/m^3.s$
T = temperature, K
t = time, s
u_t = terminal velocity, m/s
V_i = volume of phase i, m^3
w_i = mass fraction of component i
x = distance from interface in aqueous phase, m

Greek symbols

δ = film thickness $\delta = D/k_L$, m
ε_i = volume fraction of phase i
η = Kolmogoroff's length scale with averaged turbulent dissipation rate $\eta = P/V\rho_c$, m
μ_i = viscosity of component i or phase i, $mN.s/m^2$
ρ_i = density of component i or phase i, kg/m^3
σ, σ_{ij} = interfacial tension between components i, j or i, j phases, mN/m
σ_i = surface tension of component i, mN/m
Φ = interaction parameter

Dimensionless groups

Ha = Hatta number $\frac{\sqrt{Dk}}{k_L}$
Po = Power number $\frac{P}{\rho_i n^3 d_{imp}^5}$
Re = Reynolds number $\frac{d_{32} u_t \rho}{\mu}$
Re_{imp} = Impeller Reynolds number $\frac{d_{imp}^2 n \rho}{\mu}$
We = Weber number $\frac{\rho_c n^2 d_{imp}^3}{\sigma}$

Subscripts and superscripts

$*$ = value on interface ($x=0$)
aq = aqueous phase
bulk = bulk region of aqueous phase
c = continuous phase
d = dispersed phase
film = film region of aqueous phase
org = organic phase
t = total reaction system (dispersed phase + aqueous phase)
w = water

Literature Cited

1. Volkov AG. *Liquid Interfaces in Chemical, Biological and Pharmaceutical Applications*. New York, NY: CRC Press, 2001.
2. Bergbreiter DE, Sung SD. Liquid/liquid biphasic recovery/reuse of soluble polymer-supported catalysts. *Adv Synth Catal*. 2006;348(12–13):1352–1366.
3. Wirth TE. *Microreactors in Organic Synthesis and Catalysis*. Weinheim: Wiley, 2008.
4. Schofield K. *Aromatic Nitration*. Cambridge: CUP Archive, 1980.
5. Chaudhari RV, Mills PL. Multiphase catalysis and reaction engineering for emerging pharmaceutical processes. *Chem Eng Sci*. 2004; 59(22–23):5337–5344.
6. Carberry JJ. *Chemical and Catalytic Reaction Engineering*. Courier Dover Publications, 2001.
7. Levenspiel O. *Chemical Reaction Engineering*, *3rd ed*. Wiley, 1999.
8. Doraiswamy LK, Sharma MM. *Heterogeneous Reactions: Analysis, Examples, and Reactor Design, Volume 2: Fluid-Fluid-Solid Reactions*. New York, NY: Wiley-Interscience, 1984.
9. Westerterp KR, Swaaij WPMV, Beenackers AACM. *Chemical Reactor Design and Operation*, *2nd ed*. New York, NY: Wiley, 1984.
10. Quadros PA, Oliveira NMC, Baptista CMSG. Continuous adiabatic industrial benzene nitration with mixed acid at a pilot plant scale. *Chem Eng J*. 2005;108(1–2):1–11.
11. Bird RB, Stewart WE, Lightfoot EN. *Transport Phenomena*, *2nd ed*. New York, NY: Wiley, 2002.
12. Lee S, Varma A. Kinetic study of biphasic aldol condensation of *n*-butyraldehyde using stirred cell. *Chem Eng Sci*. 2013;104:619–629.
13. Danckwerts PV. *Gas-Liquid Reactions*. New York, NY: McGraw-Hill, 1970.
14. Zaldivar JM, Molga E, Alos MA, Hernandez H, Westerterp KR. Aromatic nitrations by mixed acid. Fast liquid-liquid reaction regime. *Chem Eng Process*. 1996;35(2):91–105.
15. Zaldivar JM, Molga E, Alos MA, Hernandez H, Westerterp KR. Aromatic nitrations by mixed acid. Slow liquid-liquid reaction regime. *Chem Eng Process*. 1995;34(6):543–559.
16. Bahrmann H, Hahn H, Mayer D, Frey G. *Ullmann's Encyclopedia of Industrial Chemistry: 2-Ethylhexanol*. New York, NY: Wiley-VCH, 2013.

17. McMurry J. *Organic Chemistry, 6th ed*. Belmont, CA: Thomson, 2004.
18. Nozière B, Chabert P. Abiotic C-C bond formation under environmental conditions: kinetics of the aldol condensation of acetaldehyde in water catalyzed by carbonate ions (CO32−). *Int J Chem Kinetics*. 2010;42(11):676–686.
19. Zhou GW, Kresta SM. Correlation of mean drop size and minimum drop size with the turbulence energy dissipation and the flow in an agitated tank. *Chem Eng Sci*. 1998;53(11):2063–2079.
20. Singh KK, Mahajani SM, Shenoy KT, Ghosh SK. Representative drop sizes and drop size distributions in A/O dispersions in continuous flow stirred tank. *Hydrometallurgy*. 2008;90(2–4):121–136.
21. Baldyga J, Bourne JR, Pacek AW, Amanullah A, Nienow AW. Effects of agitation and scale-up on drop size in turbulent dispersions: allowance for intermittency. *Chem Eng Sci*. 2001;56(11): 3377–3385.
22. Nanda AK, Sharma MM. Effective interfacial area in liquid-liquid extraction. *Chem Eng Sci*. 1966;21:707–714.
23. Quadros PA, Baptista CMSG. Effective interfacial area in agitated liquid–liquid continuous reactors. *Chem Eng Sci*. 2003;58(17):3935–3945.
24. Hanna GJ, Noble RD. Measurement of liquid liquid interfacial kinetics. *Chem Rev*. 1985;85:583–598.
25. Abidin MIIZ, Raman AAA, Nor MIM. Review on measurement techniques for drop size distribution in a stirred vessel. *Ind Eng Chem Res*. 2013;52(46):16085–16094.
26. Ritter J, Kraume M. On-line measurement technique for drop size distributions in liquid/liquid systems at high dispersed phase fractions. *Chem Eng Technol*. 2000;23(7):579–581.
27. Maass S, Grunig J, Kraume M. Measurement techniques for drop size distributions in stirred liquid-liquid systems. *Chem Process Eng*. 2009;30:635–651.
28. Hinze JO. Fundamentals of the hydrodynamic mechanism of splitting in dispersion processes. *AIChE J*. 1955;1(3):289–295.
29. Batchelor GK. Kolmogoroff's Theory of Locally Isotropic Turbulence. *P Camb Philos Soc*. 1947;43(4):533–559.
30. Brown DE, Pitt K. Drop size distribution of stirred non-coalescing liquid-liquid system. *Chem Eng Sci*. 1972;27(3):577–583.
31. Sechremeli D, Stampouli A, Stamatoudis M. Comparison of mean drop sizes and drop size distributions in agitated liquid-liquid dispersions produced by disk and open type impellers. *Chem Eng J. 1* 2006;117(2):117–122.
32. Doulah MS. Effect of hold-up on drop sizes in liquid-liquid dispersions. *Ind Eng Chem Fundam*. 1975;14(2):137–138.
33. van Woezik BAA, Westerterp KR. Measurement of interfacial areas with the chemical method for a system with alternating dispersed phases. *Chem Eng Process*. 2000;39(4):299–314.
34. Calderbank PH. Physical rate processes in industrial fermentation, Part I: the interfacial area in gas-liquid contacting with mechanical agitation. *Trans. Inst Chem. Eng*. 1958;36:443–463.
35. Godfrey JC, Obi FIN, Reeve RN. Measuring drop size in continuous liquid-liquid mixers. *Chem Eng Prog*. 1989;85(12):61–69.
36. Becker PJ, Puel F, Chevalier Y, Sheibat-Othman N. Monitoring silicone oil droplets during emulsification in stirred vessel: effect of dispersed phase concentration and viscosity. *Can J Chem Eng*. 2014; 92(2):296–306.
37. Paul EL, Obeng VA, Kresta SM. *Handbook of Industrial Mixing: Science and Practice*. Hoboken, NJ: Wiley-Interscience, 2003.
38. Laliberte M. Model for calculating the viscosity of aqueous solutions. *J Chem Eng Data*. 2007;52(2):321–335.
39. Santiago MD, Trambouz. P. Perfectly agitated reactors with 2 liquid phases - measurement of interfacial area by chemical method. *Chem Eng Sci*. 1971;26(1):29–38.
40. Brooks BW, Richmond HN. Phase Inversion in nonionic surfactant oil-water systems .2. drop size studies in catastrophic inversion with turbulent mixing. *Chem Eng Sci*. 1994;49(7):1065–1075.
41. Mlynek Y, Resnick W. Drop Sizes in an Agitated Liquid-Liquid System. *AIChE J*. 1972;18(1):122–127.
42. Desnoyer C, Masbernat O, Gourdon C. Experimental study of drop size distributions at high phase ratio in liquid-liquid dispersions. *Chem Eng Sci*. 2003;58(7):1353–1363.
43. Abrams DS, Prausnitz JM. Statistical thermodynamics of liquid-mixtures - new expression for excess Gibbs energy of partly or completely miscible systems. *AIChE J*. 1975;21(1):116–128.
44. Minitab. Help of Minitab 16: Minitab Inc., 2010.
45. Treybal RE. *Liquid Extraction, 2nd ed*. New York, NY: McGraw-Hill, 1963.
46. Wesselingh JA. The velocity of particles, drops and bubbles. *Chem Eng Process*. 1987;21:9–14.
47. Kronig R, Brink JC. On the theory of extraction from falling droplets. *Appl Sci Res*. 1950;2(2):142–154.
48. Johnson AI, Hamielec AE. Mass transfer inside drops. *AIChE J*. 1960;6(1):145–149.
49. Hu S, Kintner RC. The fall of single liquid drops through water. *AIChE J*. 1955;1(1):42–48.
50. Good RJ, Elbing E. Generalization of theory for estimation of interfacial energies. *Ind Eng Chem*. 1970;62(3):54–78.
51. Yaws CL. *Thermophysical Properties of Chemicals and Hydrocarbons*. Waltham, MA: Elsevier, 2009.
52. Dutcher CS, Wexler AS, Clegg SL. Surface tensions of inorganic multicomponent aqueous electrolyte solutions and melts. *J Phys Chem A*. 2010;114(46):12216–12230.
53. Vargaftik NB, Volkov BN, Voljak LD. International tables of the surface-tension of water. *J Phys Chem Ref Data*. 1983;12(3):817–820.
54. ANSYS. User's Manual to ANSYS FLUENT 14.5: ANSYS Inc., 2012.

Appendix A: Mass-Transfer Coefficient for the Dispersed Phase

The dispersed phase in a stirred tank forms droplets inside the tank. The mass-transfer coefficient for the dispersed phase is affected by the movements inside a droplet. The movements can be classified as a rigid drop having no movement, a laminar circulating drop and a turbulent circulating drop. According to the movement in the drop, different correlations have been developed.[45] To determine the type of drop movement, the diameter number (d^*) can be used as shown in Eq. A1[46]

$$d^* = d_{32}\left(\frac{{\mu_{aq}}^2}{\rho_{aq} g(\rho_{aq}-\rho_{org})}\right)^{-1/3} \tag{A1}$$

The diameter numbers in this study were 16 ± 3. With the assumption that the droplets are clean, the droplet movement in this study is evaluated as a laminar circulating drop. For this case, Kronig and Brink[47] developed the generally accepted relation as Eq. A2

$$k_L = \frac{17.9D}{d_{32}} \tag{A2}$$

Johnson and Hamielec[48] experimentally confirmed that this equation provides good estimations when the Reynolds number is below 70 for the case of *n*-butanol and cyclohexanol. The Reynolds number range in the present study was 51 ± 13, with the terminal velocity calculated from the correlation (Eq. A3) by Hu and Kintner.[49]

$$u_t = \sqrt{\frac{4gd_{32}(\rho_{aq}-\rho_{org})}{3\rho_{aq}C_D}} \tag{A3}$$

In this study, therefore, Eq. A2 was used for the mass-transfer coefficient for the dispersed phase. The Sauter mean diameter and the averaged value of nBAL and 2EHEL were used for the drop diameter and the physical properties for the organic phase, respectively.

Appendix B: Estimation of the Interfacial Tension

The interfacial tension between organic and aqueous phases has a significant role in predicting the interfacial area through stability of the organic system as the dispersed phase in this study. There are various empirical correlations to predict the interfacial tension between two liquid phases. Among these, Good and Elbing[50] suggested Eq. B1 to estimate the interfacial tension from the surface tensions of the two phases (1 – organic, 2 – aqueous)

$$\sigma_{12}=\sigma_1+\sigma_2-2\Phi_{12}\sqrt{\sigma_1\sigma_2} \quad \text{(B1)}$$

Φ_{12} is an interaction parameter which can be obtained from dipole moments using the figure available in Good and Elbing,[50] and the dipole moments for nBAL and 2EHEL obtained from Yaws,[51] the interaction parameter averaged for nBAL and 2EHEL was 0.85.

The continuous aqueous phase in this study contains significant amounts of NaOH which affect the surface tension of water. Dutcher et al.[52] provide a correlation to estimate the surface tension of inorganic multicomponent aqueous electrolyte solutions, including NaOH, which leads to Eq. B2

$$\sigma_{aq}=\sigma_w+x_{NaOH}(a_{ws}+b_{ws}T) \cdot \{a_{ws}=69.691, b_{ws}=0 \ for \ NaOH\} \quad \text{(B2)}$$

$$\sigma_w=235.8\left(\frac{647.15-T}{647.15}\right)^{1.256}\left(1-0.625\frac{647.15-T}{647.15}\right)$$

x_{NaOH} is the mole fraction of NaOH in the aqueous phase. The estimation error for the surface tension of NaOH solution was reported to be 1.3%. The surface tension of water σ_w was obtained from Vargaftik et al.[53] For the surface tension of the organic phase, surface tensions of nBAL and 2EHEL were obtained from Yaws[51] and were averaged with their mass fractions as described by Eq. B3

$$\sigma_{org}=\sum_i w_i\sigma_i; \ \sigma_{nBAL}=69.216\left(1-\frac{T}{525}\right)^{1.222}; \sigma_{2EHEL}=69.991\left(1-\frac{T}{630}\right)^{1.222} \quad \text{(B3)}$$

Appendix C: 3-D-CFD Study for P/V and the Disturbance by the Borescope

A three-dimensional (3-D) CFD technique using ANSYS FLUENT 14.5[54] was employed to check the disturbance by the borescope and to calculate the P/V (power per volume) of the 300 mL stirred tank for calculation of the continuous phase mass-transfer coefficient.

The flow disturbance by the borescope was checked through calculating the change of P/V by inserting the borescope inside the reactor. For this purpose, two meshes for the 300 mL stirred tank were prepared for the cases with or without the borescope using GAMBIT 2.4.6. Several possible cases could be evaluated because the borescope was located at the top and bottom positions and two different sized sight tubes (1/8″ and 3/16″) were also used. Among these, the bottom position with the larger 3/16″ sight tube was meshed (Figure C1) because it was expected to provide the largest effect on the reactor hydrodynamics.

The mesh was primarily hexahedral but tetrahedral mesh was also used around some parts of the cooling tube. The total mesh number was 306,160/306,856 with or without the borescope, respectively. The models used for the CFD study were RANS (Reynolds Averaged Navior Stokes), standard k-ε with standard wall function for turbulence, MRF (multiple reference frame) for impeller, Euler–Eulerian for multiphase model and continuity equation.[54] The calculations were made for the same values as in the experimental study; organic phase: 60 mL, aqueous phase: 140 mL.

Using the CFD technique, the momentum around the agitator was evaluated, and then the power was calculated (Table C1).

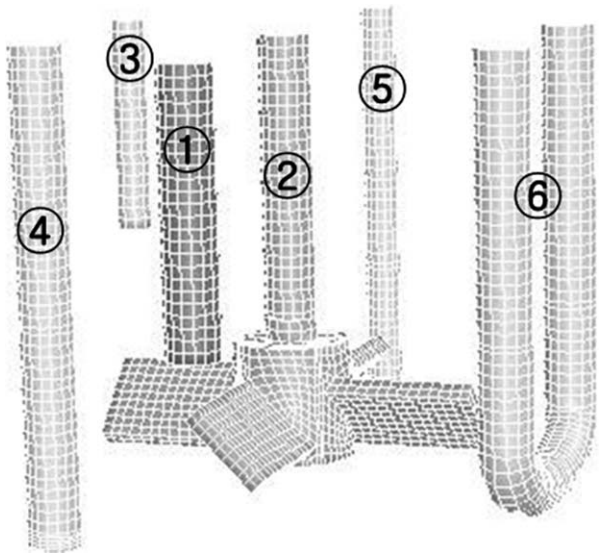

Figure C2. The mesh inside the 300 mL stirred tank reactor: the borescope (1), the agitator (2), the sample tube (3), injection nozzle (4), thermo couple (5) and the cooling tube (6).

Table C1. Comparison of P/V (W/m^3) with or Without the Borescope

rpm (min^{-1})	with borescope	without borescope	difference
600	279	276	0.8%
1000	1289	1278	0.9%

Table C2. Conversion of Agitation Speed to P/V

rpm (min^{-1})	P/V (W/m^3)
600	279
700	431
800	638
900	901
1000	1289

The agitation power with the borescope was slightly increased but, the difference with cases without the borescope was <1%. This implies that the effect of the borescope on the hydrodynamics in the reactor is negligible. This may be because there were various tubes in the reactor for sampling, injection, cooling, etc., which already served as baffles. Therefore, the borescope, with similar diameter as the other tubes, did not significantly affect the hydrodynamics.

For the calculation of the continuous phase mass-transfer coefficient, P/V as a function of rpm was calculated by the 3-D-CFD model as shown in Table C2.

Through the simulations, the power number, *Po* was about 1.22 under all operating conditions for the agitator used in the stirred tank.

Manuscript received Dec. 9, 2014, and revision received Mar. 16, 2015.